Effect of surface nano-crystallization induced by supersonic fine particles bombarding on microstructure and mechanical properties of 300M steel

Tian Zhou[a], Yi Xiong[a,b*], Zheng-ge Chen[c], Xiao-qin Zha[d], Yan Lu[a], Tian-tian He[a], Feng-zhang Ren[a,b], Harishchandra Singh[e], Jukka Kömi[f], Marko Huttula[a,e], Wei Cao[e]

[a] *School of Materials Science and Engineering, Henan University of Science and Technology, Luoyang 471023, Henan, China*

[b] *Collaborative Innovation Center of Nonferrous Metals, Luoyang 471023, Henan, China*

[c] *State Key Laboratory of Laser Interaction with Matter, Northwest Institute of Nuclear Technology, Xi'an 710024, China*

[d] *Luoyang Ship Material Research Institute, Luoyang 471000, Henan, China*

[e] *Nano and Molecular Systems Research Unit, University of Oulu, FIN-90014, Finland*

[f] *Materials and Mechanical Engineering, Center for Advanced Steels Research, University of Oulu, FIN-90014, Finland*

Abstract

Supersonic fine particles bombarding (SFPB) technology opens a new territory for engineering materials towards improved performances. Owing to its merits and emerging applications, 300M steel (tensile strength ≥ 1800 MPa) was treated with SFPB to create surface gradient nanostructures. The time dependent SFPB process was implemented on various 300M steel surface to investigate the microstructural evolution and mechanical property. 300M steel surface grains were sufficiently refined down to nanometer scale under high energy SFPB. In the subsurface layer, acicular martensite was found to be bent and broken, resulting in the high-density dislocation. At the early stage of SFPB, the impact affected area of 300M steel surface was deepened with increasing SFPB time, and the grains were constantly refined, which further lead to higher strength and improved hardness. However, after longer treatments of more than 90 s, bombardment energy accumulated at 300M steel surface resulted in grain growths and deteriorations of hardness. In particular, the newly formed microcracks substantially reduced the tensile strength. After SFPB treatment, the dimple size of the 300M steel surface fracture decreased significantly, and a large area of cleavage plane appeared, showing typical characteristics of ductile-brittle mixed fracture.

Keywords: 300M steel; Surface gradient nanostructures; Supersonic fine particles bombarding; Microstructural evolution; Mechanical properties

* Corresponding author.

E-mail address: xiongy@haust.edu.cn; Tel.: +86 135 2691 7962 (Y. Xiong)

1. Introduction

Pursuit of high- and ultra-high strength materials is an everlasting objective in structural engineering and design. In this regard, surface nanofabrication has recently been found as a new strengthen method. After surface nano-treatment, the microstructural unit size (such as grain size or lamellae thickness) of treated materials exhibit a spatial gradient, which increases gradually from nanoscale to macroscopic scale [1-3]. Gradient nanostructures can effectively avoid the performance mutation caused by the size mutation of the microstructure, which is different from the simple mixing of nano-grain, sub-micron grain and coarse grain [4-7]. It further coordinates the performance difference of different size microstructures to improve the overall service performance of such treated materials.

One of the most advanced efficient methods to create surface gradient nanostructures is supersonic fine particles bombarding (SFPB). Though SFPB is under development but it has already demonstrated its merits in various materials engineering works. Ma et al. [8] reported the surface nanostructure of 1Cr18Ni9Ti austenitic stainless steel by SFPB process and analyzed the effect of surface nano-crystallization on the tribological properties of treated 1Cr18Ni9Ti steel. The surface microstructure was successfully refined into nanocrystals followed by the strain-induced martensitic transformation. Meanwhile, the tribological properties of 1Cr18Ni9Ti steel were improved by SFPB treatment. Zhang et al. [9] also created grain refined surface layer thicker than 15 μm on low carbon steel by SFPB process. The microstructure of the surface layer was refined into fine grains with grain size of about 3 μm. Dislocation tangles and dense dislocation cells were also formed in fine grains to about 500 nm wide. Further, Kong et al. [10] treated the surface of AISI 52100 steel by SFPB process, which results in the formation of a nanocrystalline layer with thickness of about 2 μm on the treated surface. Residual compressive stress was noted on the treated surface with the maximum compressive stress on the outermost surface. The thickness of the affected region was observed to be about 60 μm. Moreover, Yang et al. [11] studied the effect of different SFPB time on the surface roughness and hardness of 18Cr2Ni4WA steel. As a result, the surface roughness was increased first and then decreased with longer duration of SFPB treatment. Meanwhile, the treated sample showed refined grains and increased hardness by SFPB treatment.

After 240s of SFPB treatment, the observed nanocrystalline layer and surface hardness were the thickest and the highest, respectively. In a nutshell, the application of SFPB process in the field of surface nanotechnology is seemingly mature. However, current research results have focused on different steels with tensile strength below 1200 MPa, such as 18Cr2Ni4WA steel. The construction of gradient nanostructures on 300M steel (≥ 1800 MPa) by SFPB method has not been reported so far. It is further crucial to investigate if such technological advancement can bring mechanical merits to ultra-high strength (UHS) steel, which are typically used in extreme conditions.

A suitable UHS target for the SFPB treatment can be the 300M steel because of the most widely used landing gear steel in the world. It possesses super high strength (≥ 1800 MPa), high transverse plasticity, high fracture toughness, excellent fatigue and corrosion resistance [12-16]. One of the potential tests to its service performance while aircraft lands and takes off is the bearing capability of the huge impact force and alternating load on the ground [17-19]. Despite these merits, the extreme harsh and repetitive working conditions require additional strengthening for the 300M steel landing gears, aiming to even longer service life and comprehensive mechanical properties.

Constructing surface strengthening layer on 300M steel can effectively improve the fatigue performance of aircraft landing gear by avoiding sudden fracture of landing gear in the harsh take-off and landing environment [20]. This also has great application prospect in military and civil aircraft manufacturing. In the present study, we created surface gradient nanostructures on UHS 300M steel via SFPB process and microstructure evolution and mechanical property variations were investigated. Followed by different time dependent treatments of 300M steel by SFPB, we systematically studied and correlated the measured properties to the microstructural changes, resulted through direct impacts from the particle bombardments. By unveiling the impact of SFPB time on the microstructure evolution and mechanical properties of the 300M, it is hoped to provide appropriate SFPB process parameters to improve the service performance of 300M steel landing gears. This work is aimed at providing the technical basis for aircraft landing gear surface structure enhancement, so as to achieve the goal of lightweight and reliable landing gear.

2. Material and methods

2.1. Material

Selected components of the 300M steel measured in wt.% were 0.38 - 0.43 C, 1.45 - 1.80 Si, 0.60 - 0.90 Mn, 0.70 - 0.95 Cr, 1.65 - 2.00 Ni, 0.05 - 0.10 V, 0.30 - 0.50 Mo, ≤ 0.35 Cu, ≤ 0.010 P and ≤ 0.010 S, with a balance Fe matrix. Before the bombarding experiment, 300M steel bars were placed in a box-type resistance furnace with a temperature of 870 ℃ for 1 h and then oil quenched. After being cooled to room temperature, it was tempered twice for holding time of 2 h at 300 ℃. It was then removed from the furnace and air-cooled to obtain a well-organized tempered martensite.

2.2. Experimental methods

300M steel bars were cut into several thin plate samples with a size of 200×60×4 mm^3 and then they were polished to have a clean surface before the SFPB treatment. To prepare 300M steel surface gradient nanostructures, these thin plate samples were divided into 6 group, and five of them were SFPB treated for 30 s, 60 s, 90 s, 120 s and 150 s, respectively. The respective treated sample are assigned as SFPB-30s, SFPB-60s, SFPB-90s, SFPB-120s and SFPB-150s, respectively. For example, SFPB-30s belongs to 300M steel surface that was treated with SFPB for 30 s. The remaining group of thin plate samples was not treated and kept as a control group. Thin plate samples was SFPB treated at room temperature, with a projectile injection distance of 10 mm, gas pressure of 1.2 MPa and gas flow rate of 10 - 30 g/s. Al_2O_3 hard particle with a particle size of 50 μm was selected as the projectile. The schematic illustration of the SFPB process is shown in Figure 1.

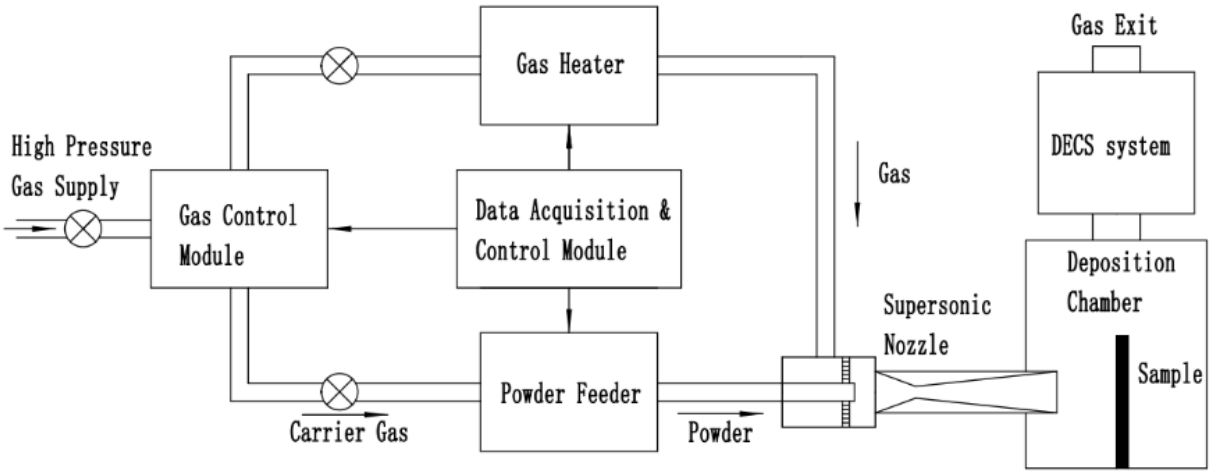

Figure 1. Schematic illustration of SFPB treatment.

The crystal structure of SFPB treated thin plate samples was analyzed by a D8 ADVANCE X-ray diffractometer (XRD) in step scan mode with a step size of 0.02° and angular range 40° - 100°. The average grain size of the sample surface layer can be obtained via simplified Williamson-Hall relation [21,22], as presented by equation (1) below as:

$$\beta\cos\theta=\varepsilon(4\sin\theta)+k\lambda/D \quad (1)$$

here $\beta\cos\theta$ is Y, $4\sin\theta$ is X, and $k\lambda/D$ is the Y-intercept, in an analogy to the linear equation relation: Y=mX+c. β is the FWHM in radians, k = 0.9, λ = 0.154056 nm is the wavelength of X-ray source, D is the grain (crystallite) size and θ is the peak position in radians.

Cross sections of the SFPB treated thin plate samples were polished and then corroded by 4% nitric acid alcohol solution for 3 - 5 s. The surface gradient nanostructure of thin plate samples was measured by a JSM-IT200 scanning electron microscope (SEM) at an accelerating voltage of 20 kV. Electron back scatter diffraction (EBSD) was also used to characterize the gradient nanostructures on the 300M steel surface layer. For the transmission electron microscopy (TEM) measurement, thin sheets were taken from the surface, subsurface and core of the thin plate samples though Gatan 691 ion thinning instrument. Then the microstructure of these thinned samples was obtained by JEM-2010 TEM.

Surface hardness of thin plate samples treated with SFPB for different treatment time was measured by a MH-3 microhardness tester under 100 g weight load and 10 s loading time. To obtain

an accurate hardness, each group of thin plate samples was measured five times. In particular, the hardness from surface to core of 300M steel samples subjected to 90 s SFPB was measured by Nano Indenter G200. Tensile samples were cut on each group of thin plate samples, as shown in Figure 2. The mechanical properties of these samples were tested at a loading speed of 0.5mm/min by Instron 5587 tensile testing machine. At least five tensile samples were prepared for each group of thin plate samples to ensure the reliability of the measured results. After that, the tensile fracture morphology of samples was tested by JSM-IT200 scanning electron microscope.

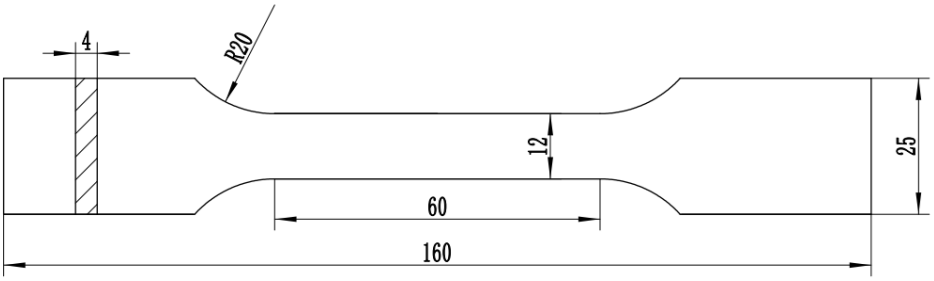

Figure 2. Schematic diagram of tensile sample dimensions (mm).

3. Results

3.1. SEM observations

SEM images of 300M steel surface gradient nanostructures created by various SFPB time are shown in Figure 3. At the initial state of SFPB, the core remains as an acicular tempered martensite structure (Figure 3a), as the energy of high-frequency impact could not reach the core area of the thin plate sample. For SFPB-30s i.e. after 30 s of SFPB treatment, the surface layer of thin plate sample subjected to severe projectile impact produces a plastic deformation induced hardened layer. Meanwhile, the energy of the high frequency impact gradually goes deeper into the subsurface layer of the thin plate samples and lead to the local deformation of the subsurface microstructure to form a deformation layer (Figure 3b). As visible, surface gradient nanostructures of 300M steel created by SFPB treatment include three regions namely hardened surface layer, deformed subsurface layer and the core matrix structure. Similar microstructure was also reported for AISI 52100 steel after

SFPB treatment [10]. With increasing SFPB treatment time, the depth of the impact affected area gradually deepens (Figures 3c and 3d).

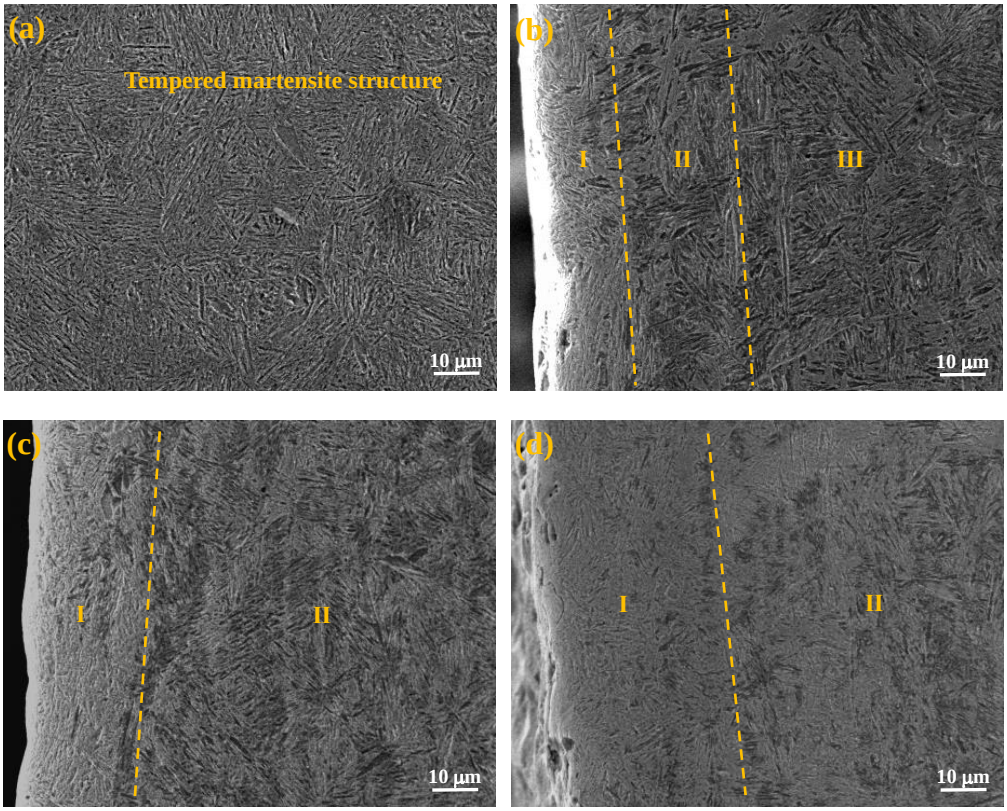

Figure 3. SEM images of the microstructure of 300M steel in (a) unaffected core and surface layer subjected to (b) 30 s; (c) 90 s and (d) 150 s SFPB treatment. (I: hardened surface layer; II: deformed subsurface layer; III: core matrix structure)

Further, the gradient nanostructure of 300M steel was characterized by EBSD and obtained results are demonstrated in Figure 4. As can be seen in the grain orientation map, grains of 300M steel are significantly broken into fine equiaxed grains in the hardened surface layer due to high-energy particle impact. As it goes deeper, the impact energy is not enough to completely break the grain, but sufficient to bend and break part of the martensite structure. The microstructure of the 300M steel core was not affected by the impact and still retained the acicular tempered martensite structure (Figure 4a). Local misorientation map in the Figure 4b qualitatively reflects the plastic deformation level of 300M steel subjected to SFPB treatment. In the 300M steel surface layer, the degree of plastic deformation is very high. With the increasing depth, the impact energy attenuation leads to the decrease of the deformation level of the microstructure. Deep into the core, almost no

deformation is observed. Figure 4c shows the boundary distribution map of 300M steel subjected to SFPB treatment. The black and green lines represent high angle grain boundaries (HAGBs) and low angle grain boundaries (LAGBs), respectively. In general, the boundaries of adjacent grains whose phase difference is less than 10° are LAGBs. On the contrary, grain boundaries with phase difference greater than 10° are HAGBs. The LAGBs of the 300M steel surface layer accounts for more than 60% of the total, and the subgrain boundaries with a phase difference of less than 2° accounts for 45%. They play an important role in the formation of nanocrystals. During SFPB process, the severe plastic deformation of the 300M steel surface layer promotes the proliferation, rearrangement, and annihilation of dislocations, which all together lead to the generation of a large number of dislocation cells and walls (Figure 5a and 6e). These dislocations further developed into LAGBs and gradually transformed into HAGBs, which further promote the formation of ultrafine grains and nanocrystalline structures. A similar phenomenon was also reported in the surface nano-crystallization of 17-4 precipitation-hardening stainless steel [23]. The inverse pole figure analysis of 300M steel subjected to SFPB shows that the grain orientation in the impact affected area is dominated by <001> (Figures 4d). The maximum texture value (3.77) is found to correspond to the <001> texture, indicating heavy deformation in the impact affected area.

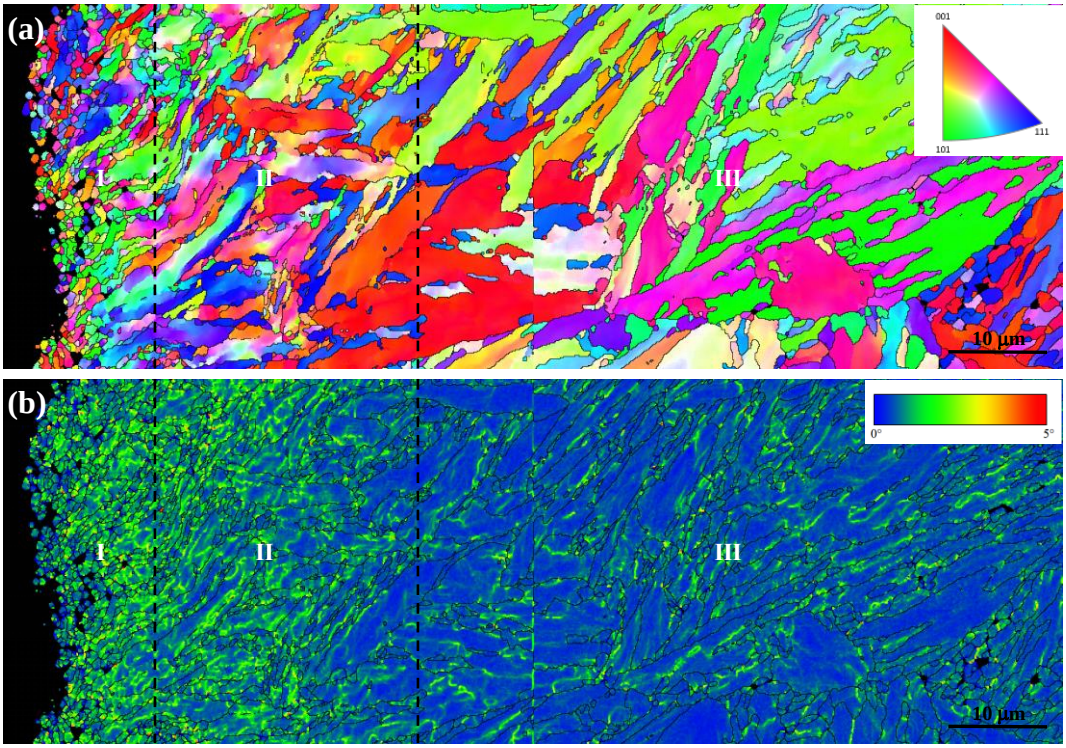

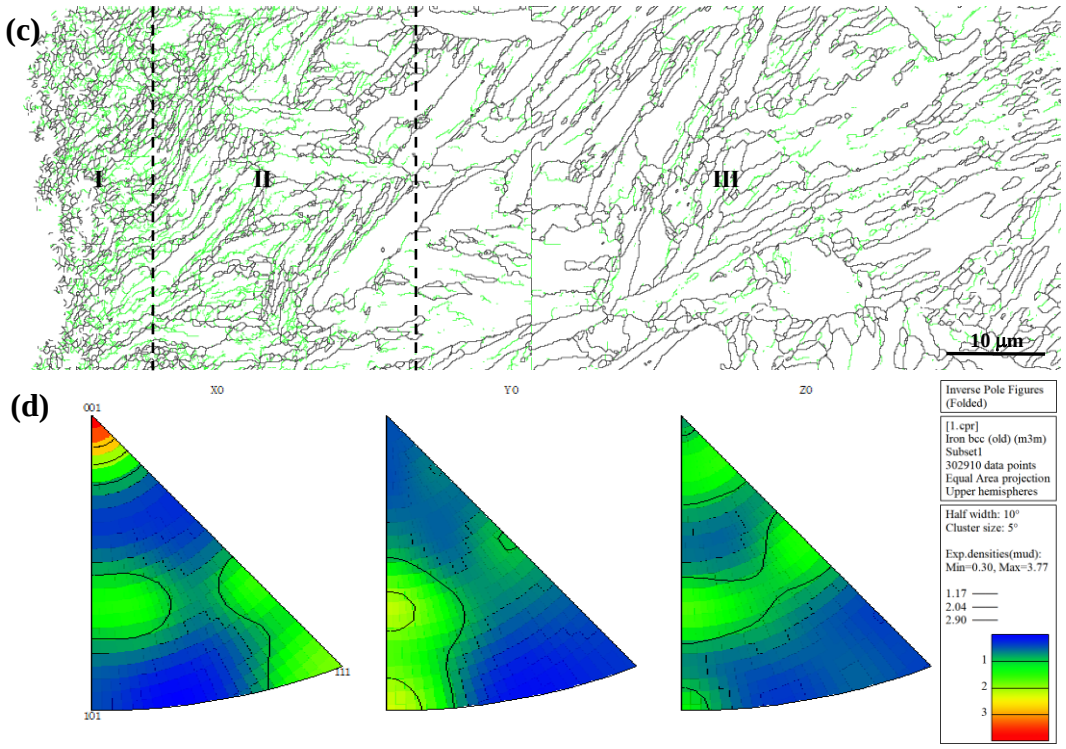

Figure 4. Grain orientation map (a), local misorientation map (b), boundary distribution map (c) and the IPF (d) of 300M steel subjected to SFPB. (I: hardened surface layer; II: deformed subsurface layer; III: core matrix structure)

3.2. TEM observations

TEM images of 300M steel hardened surface layer for SFPB-60s and SFPB-120s are shown in Figure 5. During SFPB process, sufficiently large number of dislocations resulting from plastic deformation turned out at the treated steel surface. These dislocations continuously entangled and plugged each other and formed many dislocation cells (Figure 5a and 5b). High density dislocation cells were also reported in the low carbon steel subjected to SFPB treatment [9]. As the energy accumulates on the surface, the dislocation motion gains enough momentum. Dislocation interaction and rearrangement gradually form a low energy dislocation network, which results in the formation of dislocation cells and walls with a clear subgrain boundary [24]. The subgrain boundaries grew gradually through the migration and the dislocation density in the subgrain decreases further. Figures 5c and 5d shows the bright field and dark field images of 300M steel hardened surface layer SFPB-60s, respectively. A fine subgrain in the hardened surface layer can be clearly noted. By conducting selective area electron diffraction (SAED, Figure 5d), the circular

diffraction spots indicate that the grains have been significantly refined to the nanometer scale. Similar diffraction rings have also been reported in 1Cr18Ni9Ti and AISI 52100 steel subjected to SFPB treatment [8,10]. Figures 5e and 5f shows the bright field and dark field images of 300M steel hardened surface layer for SFPB-120s i.e. sample treated by 120 s SFPB, respectively. Compared with SFPB-60s, the hardened surface layer of SFPB-120s owns a higher degree of grain refinement, and the diffraction ring in the SAED pattern is relatively continuous and clearer. However, a small number of grains tend to grow up, which found to be related to the accumulation of surface impact energy. High resolution TEM images of SFPB treated samples show clear dislocation lines (Figure 5g) and ε-carbides (Figure 5h). Liu et al. [25] confirmed that the precipitated phase of 300M steel is mainly ε-carbides. The formation of the ε-carbide may be traced to the supersaturation of martensite with carbon leading to the generation of internal stresses, and lattice relaxation occurring via the precipitation of carbides. These dispersed fine ε-carbides usually have a positive effect on the mechanical properties of the treated material, enhancing the 300M steel microstructure.

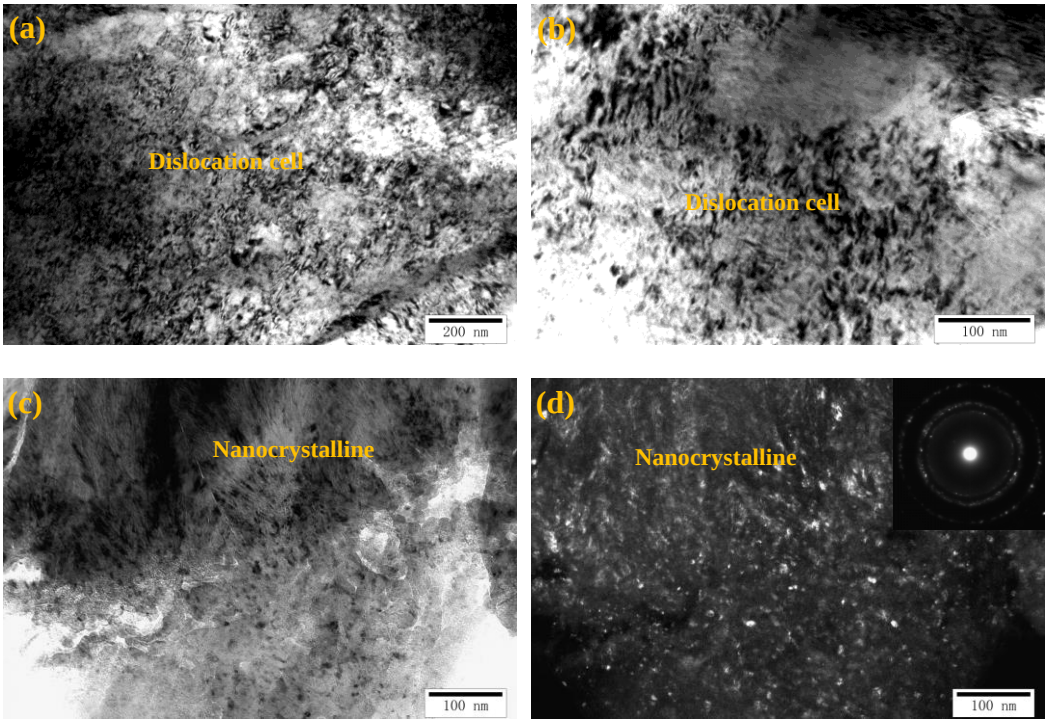

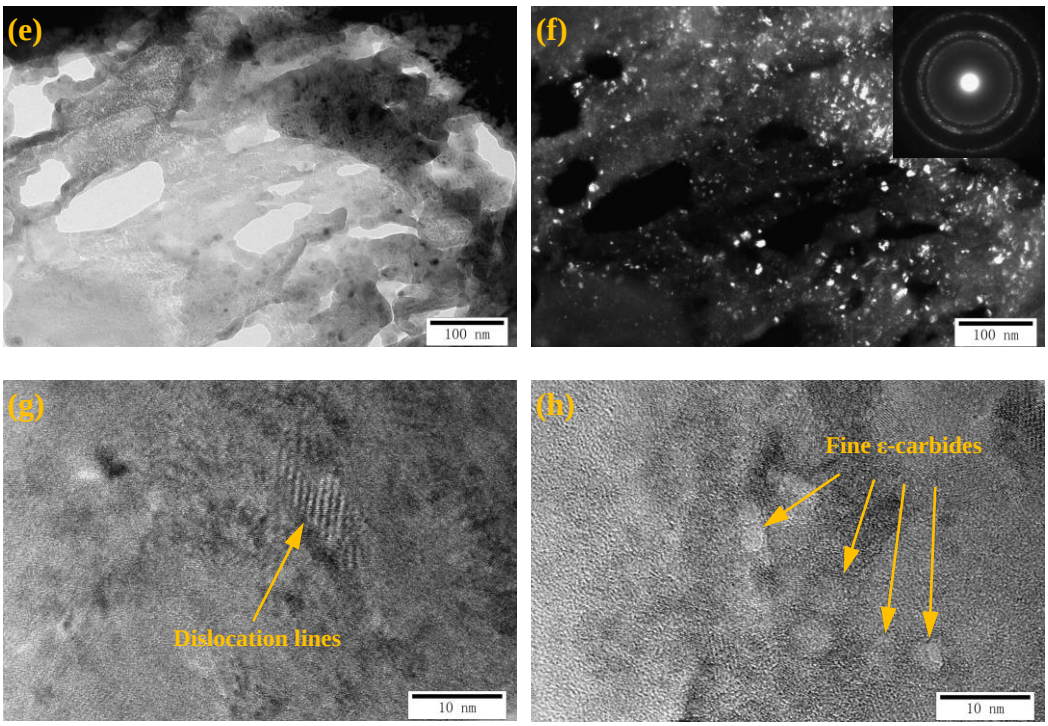

Figure 5. TEM observed hardened surface layer microstructure of 300M steel subjected to (a, b, c, d) 60 s and (e, f, g, h) 120 s SFPB.

TEM images of subsurface layer (50 μm below the surface) of 300M steel for SFPB-60s and SFPB-120s are shown in Figure 6. After being absorbed by 300M steel surface layer, the kinetic energy of the particles transferred to subsurface layer became lower. Therefore, for SFPB-60s, 300M steel subsurface layer remains the large and interlacing acicular tempered martensite structure, as shown in Figures 6a and 6b. For SFPB-120s, lower impact energy causes the subsurface acicular tempered martensite structure to bend and break (see Figures 6c and 6d). During SFPB process, the high-density dislocations in the subsurface microstructure were entangled and piled up, and as a result of violent interaction between dislocation and grain boundary, formation of dislocation wall was observed [26,27], as noted in Figures 6e and 6f. Compared with the hardened surface layer, the degree of grain refinement in the subsurface layer is lower. After SFPB treatment, 300M steel surface shows a gradient change in the microstructure from surface to subsurface and then to the core.

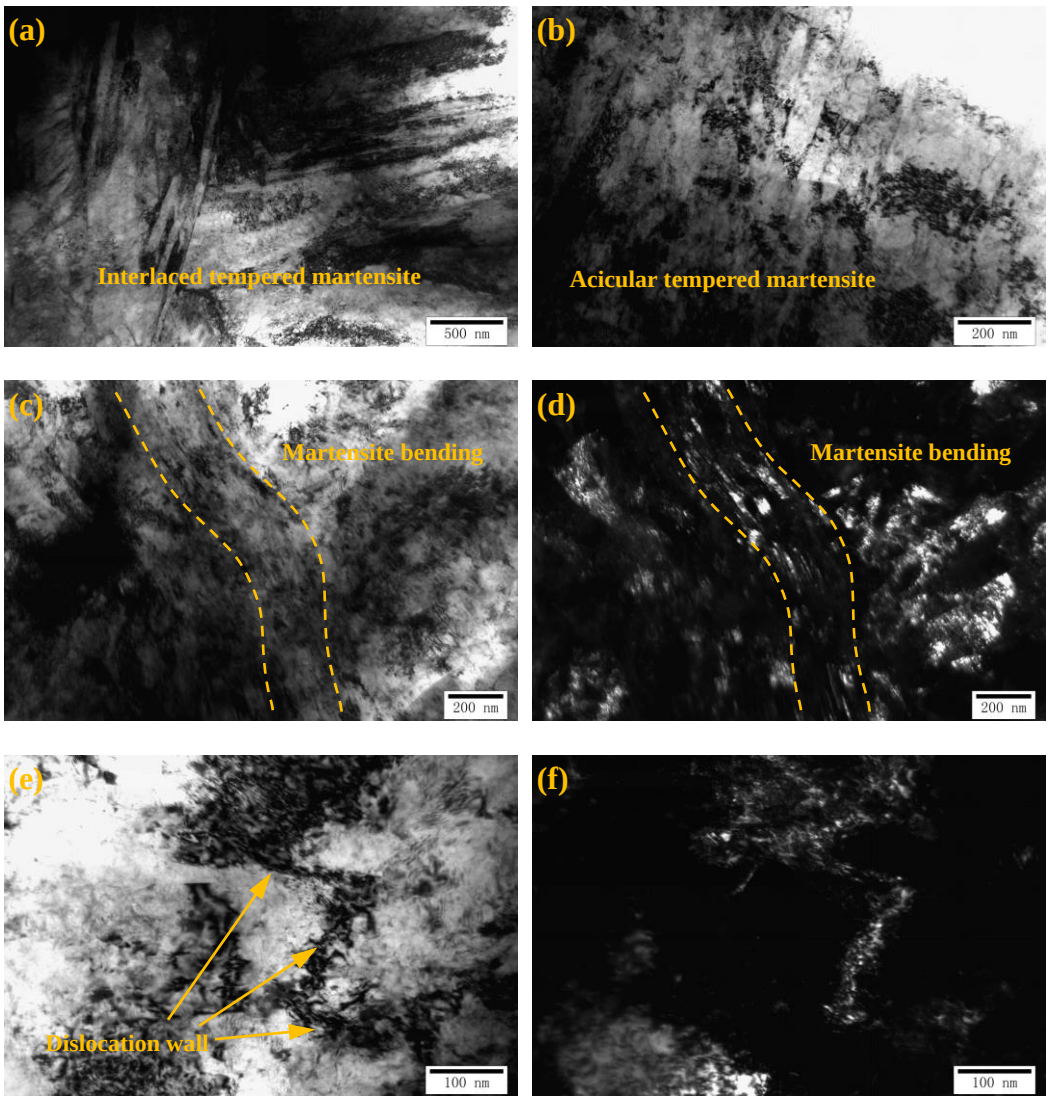

Figure 6. TEM observed subsurface microstructure of 300M steel at 50 μm below surface subjected to (a, b) 60 s and (c, d, e, f) 120 s SFPB treatments.

3.3. Surface integrity

Surface morphology of 300M steel subjected to various SFPB time is shown in Figure 7. 300M steel surfaces without SFPB treatment have shallow polishing scratches (Figure 7a). After SFPB treatment, 300M steel sample surface undergoes plastic deformation under particle impact, resulting in a large number of impact pits (Figures 7b - 7f). This leads to a significant increase in the surface roughness of 300M steel, which is in line with a previous report [11]. When the particles repeatedly bombarded at the same place of the 300M steel surface, honeycombed pits are formed (Figure 7b). This is because after the initial stage of surface hardening, subsequent impact only

produces a slight plastic deformation on the surface and results in honeycombed pits. The size change of honeycomb pits on the 300M steel surface is consistent with the trend of its surface hardness (see Figure 9). The highest surface hardness of SFPB-90s coincides with its smallest pit size (Figure 7d). It is noteworthy to mention that for SFPB-120s, microcracks were formed on the surface of the 300M steel (Figure 7e). As the SFPB treatment time increased to 150 s, the initiation and propagation of cracks become more intensive, and the density and depth of surface crack showed a massive increase. Meanwhile, the lamellar structure appears to be significantly stable on the 300M steel surface after being impacted for a longer time (see Figure 7f). During the continuous impact, the deformation of the hardened surface layer seems more resistive than at the beginning. Further, the stress accumulates on the surface of the treated sample and induces the initiation and propagation of microcracks because of longer time treatment [28,29].

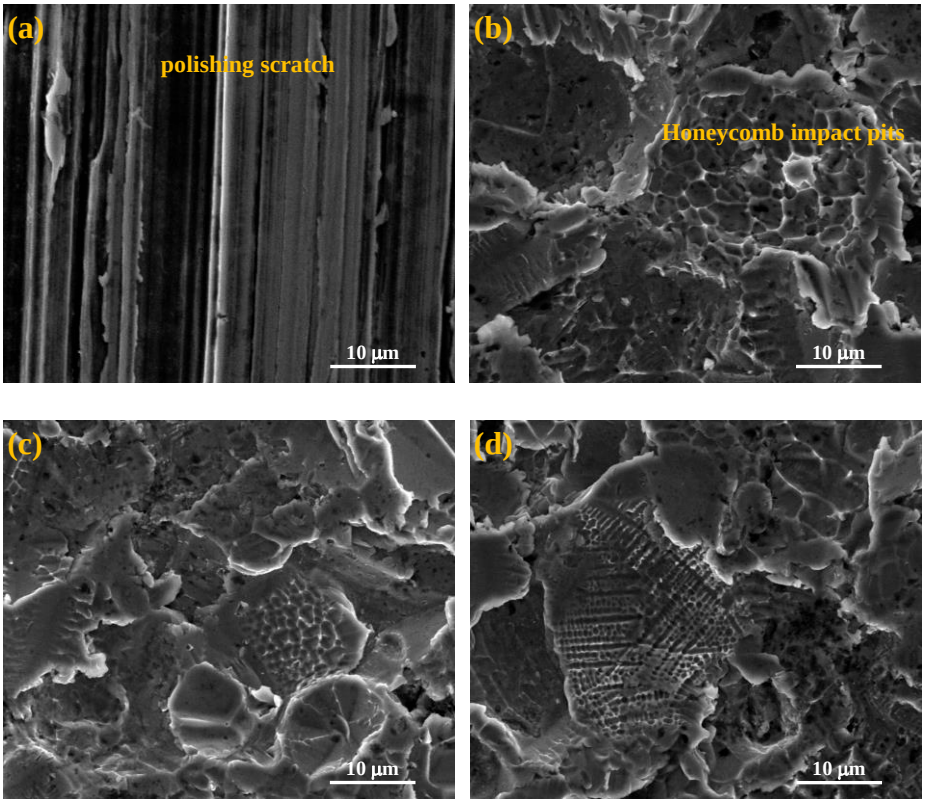

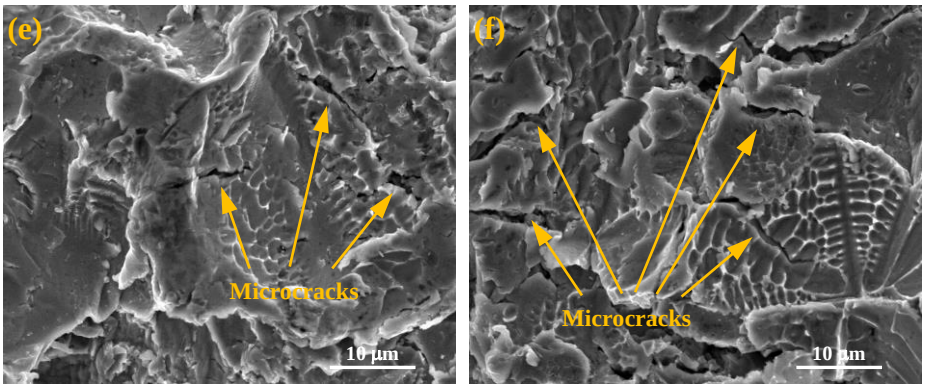

Figure 7. SEM images of 300M steel surface (a)untreated and subjected to (b)30 s; (c)60 s; (d)90 s; (e)120 s; (f)150 s SFPB.

3.4. XRD evolutions

Figure 8 shows the diffraction pattern of 300M steel subjected to various SFPB treatment time. The pattern shows three visible diffraction peaks of ferrite, namely (110), (200) and (211). The diffraction peak intensity of (110) reflection of untreated sample shows the highest intensity and minimum peak width (i.e. FWHM). After sequential SFPB treatment, the intensity of the diffraction peak decreases and the peak width get broader. Broadening degree of XRD peak is related to the grain size. The smaller grains diffract X-rays into larger distributions [10,30]. Broadening in the diffraction peak confirms that the SFPB treatment resulted in a significant refinement of 300M steel surface grains.

According to Williamson-Hall relation (equation (1)), the average surface grain size of 300M steel subjected to SFPB is reduced to the nanometer scale, which is less than 20 nm (Figure 8). With the increase in SFPB time, the average grain size of 300 M steel surface layer decreases first and then increases. This is because, in the initial stage of SFPB process, the bombardment of high-energy particles continuously crushed the martensite structure at the 300M steel surface layer and refined the grains. Subsequently, the prolonged bombardment causes energy to accumulate on the surface of the sample, and thermo-mechanical coupling caused by ultrasonic frequency impact leads to the grain recovery. By magnifying the diffraction peak of the crystal plane (110), the peak position shifts to the right and the diffraction angle increases after SFPB treatment. This is due to the formation of residual compressive stress on the 300M steel surface layer caused by ultrasonic

frequency impact, resulting in the possible lattice distortion that shifts the diffraction peak to a higher angle. Residual compressive stress can be formed on the sample surface through SFPB treatment, which also matches with the results of Kong et al. [10].

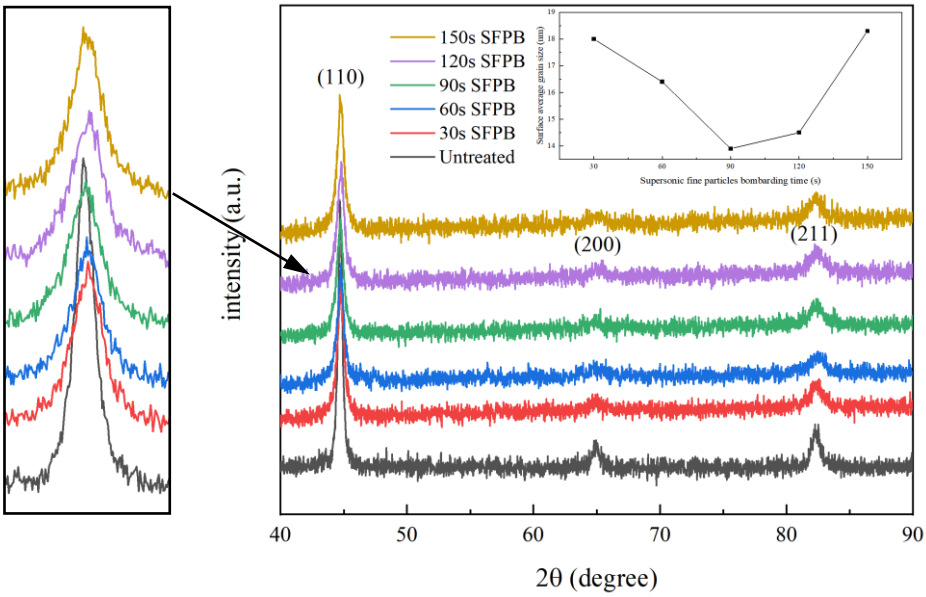

Figure 8. X-ray diffraction patterns of 300M steel subjected to various SFPB times.

3.5. Mechanical properties

Figure 9 shows the stress-strain curves of 300M steel subjected to various SFPB treatment time. Strength and grain size of the treated material typically follow the Hall-Petch relationship [31,32]. At the early stage of SFPB, the strength of 300M steel first increases with the increase of SFPB time. This trend in strength is also related to the change of surface grain size and impact affected area. Notably, after SFPB time exceeded to 90 s, the tensile strength of 300M steel decreases sharply. Over a long period of high energy impact, microcracks can form on the 300M steel surface (Figures 7e and 7f). During the tensile test, the stress concentration at the microcrack tip results in the real stress far exceeding the apparent stress [33,34]. At low experimental stress levels, microcracks can also spread over 300M steel samples and may result in fracture. The strength variation trend of 300M steel subjected to various SFPB time is shown in Figure 10. For SFPB-90s, the tensile strength of 300M steel reaches the maximum value of 1906 MPa.

Surface hardness of 300M steel subjected to various SFPB time is shown in Figure 10. With SFPB time, the surface hardness of 300M steel increases first and then decrease. During SFPB process, plastic deformation occurs at 300M steel surface due to high energy impact. Accumulation of large number of dislocations on the surface layer of 300M steel leads to the work hardening phenomena. Meanwhile, the surface layer grains are broken and refined under the action of high energy impact, which results in the effect of fine grain strengthening [35]. The combined effect of these two hardening mechanisms increases the surface hardness of 300M steel. For SFPB-90s, 300M steel's surface hardness reaches the maximum HV to 803, which is 46% higher than the original value of 550. With further extension of SPFB time, the accumulation of surface bombardment energy promotes grain recovery and result in a slight decrease in the 300M steel's surface hardness. XRD analysis of 300M steel samples subjected to different time of SFPB treatment also confirms this argument. In particular, the nano-indentation hardness of 300M steel subjected to 90 s SFPB at different layer depths is shown in Figure 11. With the increase in layer depth of 300M steel, the nano-indentation hardness gradually decreases, which is consistent with the observation of the gradient nanostructure (Figure 4).

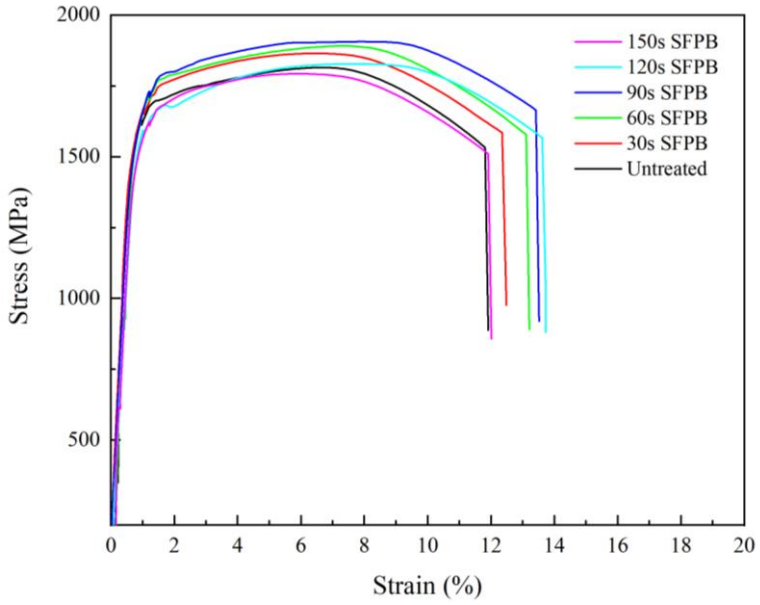

Figure 9. Stress-strain curves of 300M steel subjected to various SFPB times.

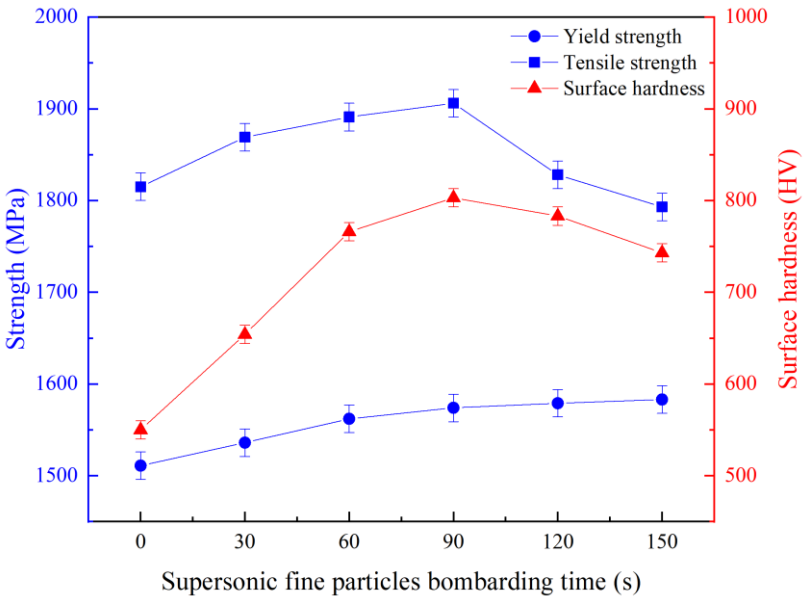

Figure 10. Strength and surface hardness of 300M steel subjected to various SFPB times.

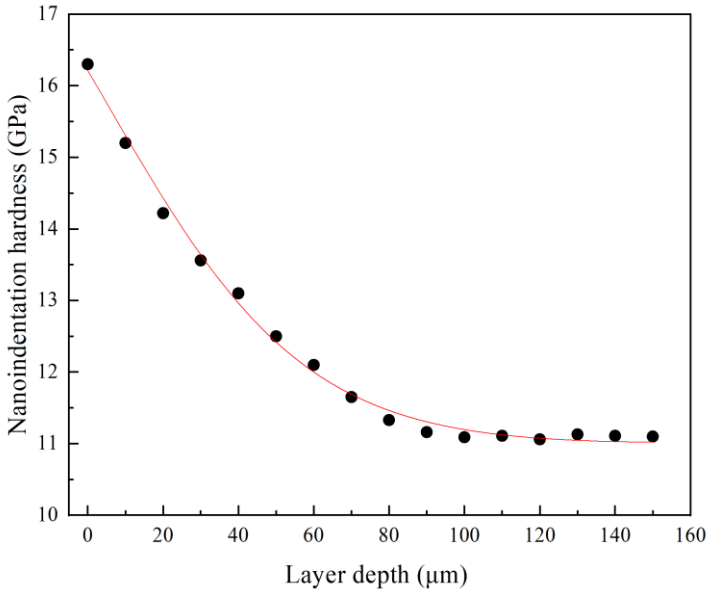

Figure 11. Nano-indentation hardness of 300M steel subjected to 90 s SFPB at different layer depths.

3.6. Tensile fracture morphology

Tensile fracture morphology of 300M steel subjected to various SFPB time is shown in Figure 12. In the undeformed core region, the tensile fracture has large and deep dimples and shows typical ductile fracture characteristics (Figure 12a), as the high energy impact causes grain refinement and dislocation increment, thus hindering the plastic deformation. In the surface layer, grain refinement

caused by high energy impact greatly reduces the dimple size and produces a large area of cleavage plane [36]. Therefore, the surface layer fracture shows the characteristics of ductile-brittle mixed fracture. Limited by the characteristics of SFPB process, the particles carried by high speed airflow cannot impact evenly to each area of 300M steel surface. This indicates the possible existence of remaining large grains in some areas on the 300M steel surface layer, which leads to some dimples in the surface layer fracture morphology (Figures 12b and 12f). By comparing the tensile fracture, morphology of treated samples under various SFPB time shows that the depth of impact affected area increases gradually with the increase in SFPB time.

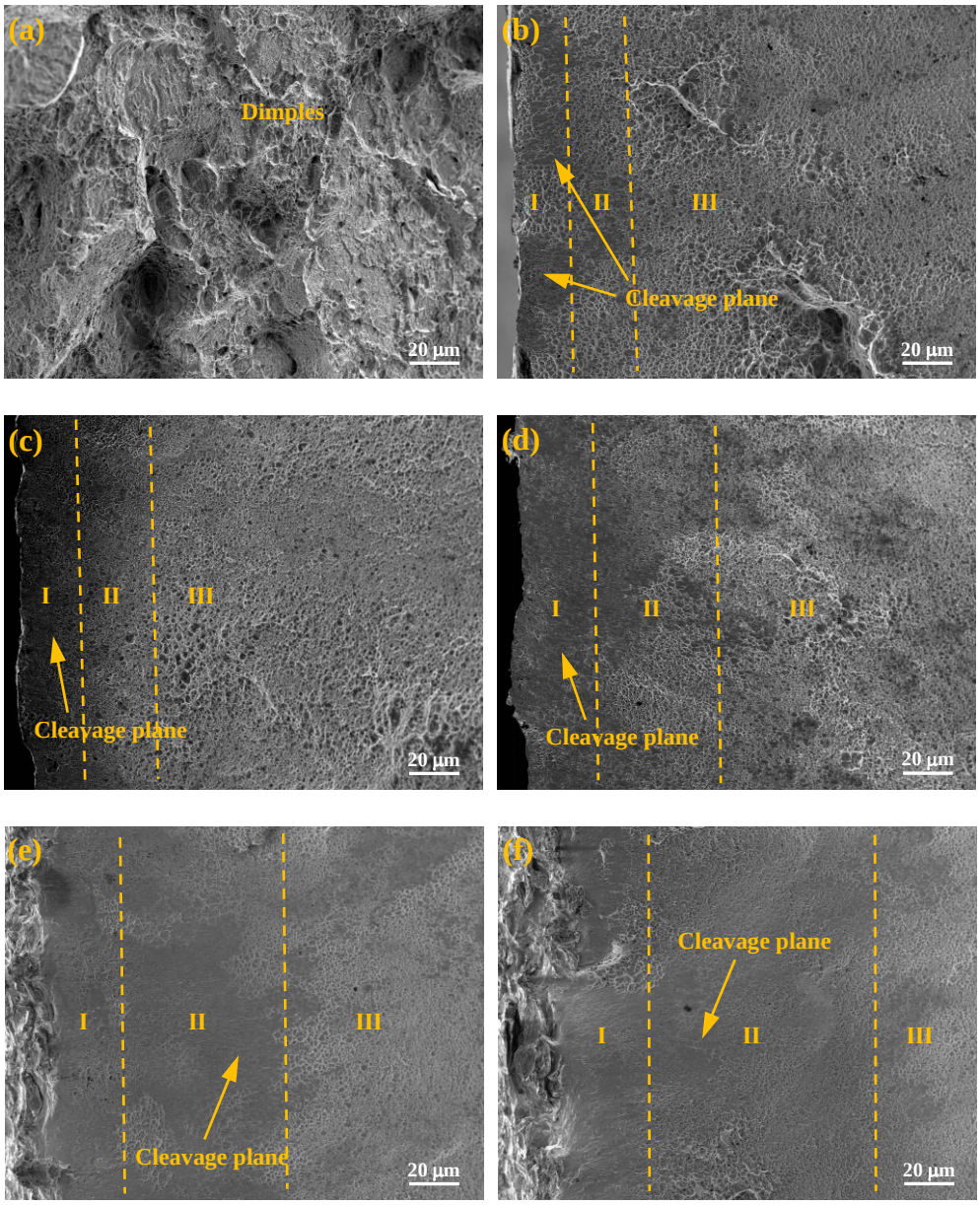

Figure 12. Tensile fracture morphology of 300M steel in (a) unaffected core and impact affected area subjected to (b) 30 s; (c) 60 s; (d) 90 s; (e) 120 s and (f) 150 s SFPB treatment. (I: hardened surface layer; II: deformed subsurface layer; III: core matrix structure)

4. Discussion

SFPB process, in general, strengthen the 300M steel surface layer by constructing gradient nanostructures. After SFPB treatment, the created gradient microstructure of 300M steel surface has been divided into three regions from surface to core as hardened surface layer, deformed subsurface layer and core matrix structure (Figure 4a). Under the action of high-energy impact, severe plastic deformation occurs at 300M steel surface to form a high-density dislocation (Figure 5a). The energy accumulation on the surface layer provides sufficient driving force for dislocation movement and causes dislocation rearrangement to form a large number of tiny dislocation cells. With such continuous dislocation movement, LAGBs gradually transform into HAGBs to promote the formation of nanoscale grains (Figure 4c). Dislocation motion has been found to be the dominant nano-crystallization mechanism. This mechanism was also confirmed by Liu et al. in their investigation of surface nano-crystallization [23].

The grain size of the hardening layer of 300M steel surface is greatly refined and show the refinement up to 10 nm (Figures 5d and 5f). The improvement in the performance of treated material is dominated by grain refinement strengthening in the hardening layer. After absorption by 300M steel surface layer, the bombardment energy gradually decreases. In the subsurface layer, the bombardment energy is not enough to create fully nanometer scale acicular tempered martensite structure and can only bend and break the same (Figures 6c and 6d). As a result, large number of dislocation walls are formed by dislocation entanglement and accumulation caused by plastic deformation (Figures 6e and 6f). The work hardening effect among them plays a key role in the deformed subsurface layer of treated steel surface. The core microstructure of treated steel was not affected by SFPB process and retains the original tempered martensite structure. Successive gradient nanostructure from the surface to the core harmonizes the mechanical properties of the different size microstructure and improves the overall mechanical properties of the steel. Observed results show good agreement with previous reports, wherein tribological properties, corrosion

resistance and fatigue life of the materials were reportedly improved by SFPB process [8,9,20].

SFPB time shows significant effect on the microstructure and mechanical properties of constructed gradient nanostructures of 300M steel. With the increase in time of SFPB, the depth of the gradient nanostructure of treated steel surface increases. For SFPB-30s, the depth of the impact affected zone reaches to about 20 μm (Figure 12b). For SFPB-150s i.e. when the SFPB time increased to 150 s, the depth of impact affected area also increases to 120 μm (Figure 12f). TEM results of subsurface layer (50 μm below the surface) for SFPB-60s and SFPB-120s also confirm this trend. The original tempered martensite structure is still retained at 50 nm below the surface of steel for SFPB-60s (Figures 6a and 6b). However, for SFPB-120s i.e. when SFPB time increases to 120 s, the martensite in this depth begins to bend and break (Figures 6e and 6f). The reduction of the nanocrystalline grain size on 300M steel surface layer is the result of continuous development of substructures (dislocation cells and subgrains) formed by high-energy impact. With the further extension in SFPB time, the increase in the size of surface nanocrystalline grains can be attributed to the grain recovery caused by the accumulation of the bombardment energy. Different SFPB time changes the surface hardness and strength of 300M steel. The surface hardness and strength of steel subjected to SFPB increase first and then decrease with the increase in SFPB time (Figure 10). This trend in change of the mechanical properties of 300M steel is consistent with the change in the microstructure. It is worth noting that when the SFPB time exceeds to 90 s, the tensile strength of the 300M steel has dropped significantly. This is caused by the formation of microcracks on the surface of 300M steel due to prolonged high-energy impact (Figures 7e and 7f). During the tensile test, the stress of the material is concentrated on the tip of the surface microcracks, so that the lower experimental stress level can also induce the unstable fracture of the steel [34,35]. Meanwhile, SFPB treatment has also changed the tensile fracture morphology of 300M steel, and its fracture morphology has changed from ductile fracture to ductile-brittle mixed fracture (Figures 12a -12f).

5. Conclusion

To conclude, 300M steel surface was treated by supersonic fine particles bombarding process to create gradient nanostructures, and the effect of bombardment time on the microstructure evolution and mechanical properties was thoroughly investigated. The following conclusions are

drawn:

1. After SFPB treatment, the microstructure at the 300M steel surface presents spatial gradient. In the hardened surface layer, the grains are fully refined to nanocrystals under high energy impact. The subsurface acicular tempered martensite structure is bent and broken during the SFPB process. However, the core still retains the original tempered martensite structure.
2. With the increase in SFPB time, the depth of impact affected area of 300M steel increases gradually. Meanwhile, the strength and surface hardness of 300M steel first increase and then decrease under the influence of changes in the microstructure. After the SFPB time exceeded to 90 s, the tensile strength of 300M steel has dropped sharply due to surface microcracks. After 90 s SFPB treatment, which also found to be the best SFPB treatment time, 300M steel has tensile strength of 1906 MPa, yield strength of 1582 MPa and surface hardness of HV 803.
3. Post SFPB treatment, 300M steel core fracture has been found to show a large and deep dimple, showing ductile fracture characteristics. In the surface layer fracture, the dimple size decreases, and a large area of cleavage plane appears, which further present the characteristics of ductile-brittle mixed fracture.

Acknowledgment

This work was supported by the National Natural Science Foundation of China [grant numbers U1804146 and 52111530068]; the Program for Science, Technology Innovation Talents in Universities of Henan Province [grant number 17HASTIT026]; the Education Department of Henan Province [grant number 16A430005]; the Science and Technology Innovation Team of Henan University of Science and Technology [grant number 2015XTD006]; the Foreign Experts Introduction Project of Henan Province [grant number HNGD2020009]; and the Academy of Finland [grant number 311934].

References

[1] Ye, C., Telang, A., Gill, A. S., Suslov, S., Idell, Y., Zweiacker, K., Wiezorek, J. M. K., Zhou, Z., Qian, D., Mannava, S. R., & Vasudevan, V. K. (2014). Gradient nanostructure and residual stresses induced by ultrasonic nano-crystal surface modification in 304 austenitic stainless steel for high strength and high

ductility. Materials Science and Engineering: A, 613(8), 274-288.

[2] Pour-Ali, S., Kiani-Rashid, A. R., Babakhani, A., & Virtanen, S. (2018). Severe shot peening of AISI 321 with 1000 % and 1300 % coverages: A comparative study on the surface nanocrystallization, phase transformation, sub-surface microcracks, and microhardness. International Journal of Materials Research, 109(5), 451-459.

[3] Wang, R., Zheng, Z., Zhou, Q., & Gao, Y. (2016). Effect of surface nanocrystallization on the sensitization and desensitization behavior of Super304H stainless steel. Corrosion Science, 111, 728-741.

[4] Thevamaran, R., Lawal, O., Yazdi, S., Jeon, S. J., Lee, J. H., & Thomas, E. L. (2016). Dynamic creation and evolution of gradient nanostructure in single-crystal metallic microcubes. Science, 354(6310), 312-316.

[5] Deng, S. Q., Godfrey, A., Liu, W., & Hansen, N. (2016). A gradient nanostructure generated in pure copper by platen friction sliding deformation. Scripta Materialia, 117, 41-45.

[6] Lei, Y. B., Wang, Z. B., Xu, J. L., & Lu, K. (2019). Simultaneous enhancement of stress- and strain-controlled fatigue properties in 316L stainless steel with gradient nanostructure. Acta Materialia, 168, 133-142.

[7] Li, J., Weng, G. J., Chen, S., & Wu, X. (2017). On strain hardening mechanism in gradient nanostructures. International Journal of Plasticity, 88, 89-107.

[8] Ma, G., Xu, B., Wang, H., Si, H., & Yang, D. (2011). Effect of surface nanocrystallization on the tribological properties of 1Cr18Ni9Ti stainless steel. Materials Letters, 65(9), 1268-1271.

[9] Zhang, L., Ma, A., Jiang, J., Song, D., Yang, D., & Chen, J. (2013). Electrochemical corrosion properties of the surface layer produced by supersonic fine-particles bombarding on low-carbon steel. Surface and Coatings Technology, 232, 412-418.

[10] Kong, L., Lao, Y., Xiong, T., & Li, T. (2013). Nanocrystalline surface layer on AISI 52100 steel induced by supersonic fine particles bombarding. Journal of Thermal Spray Technology, 22(6), 1007-1013.

[11] Yang, Y., Cui, X., Zhao, X., Dong, M., Zhou, J., & Jin, G. (2020). Surface nanocrystallized structural steel with enhanced tribological properties under different sliding conditions. Wear, 460-461, 203429.

[12] Jing, G. Y., Huang W. P., Yang H. H., & Wang, Z. M. (2020). Microstructural evolution and mechanical properties of 300 M steel produced by low and high power selective laser melting. Journal of Materials Science & Technology, 48, 44-56.

[13] Liu, F., Lin, X., Yang, H., Wen, X., Li, Q., Liu, F., & Huang, W. (2017). Effect of microstructure on the fatigue crack growth behavior of laser solid formed 300M steel. Materials Science and Engineering: A, 695, 258-264.

[14] Bag, A., Delbergue, D., Bocher, P., Lévesque, M., & Brochu, M. (2018). Statistical analysis of high cycle fatigue life and inclusion size distribution in shot peened 300M steel. International Journal of Fatigue, 118, 126-138.

[15] Zhao, W., Liu, D., Zhang, X., Zhou, Y., Zhang, R., Zhang, H., & Ye, C. (2018). Improving the fretting and corrosion fatigue performance of 300M ultra-high strength steel using the ultrasonic surface rolling

process. International Journal of Fatigue, 121, 30-38.

[16] Guo, Q., Liu, J. H., Yu, M., & Li, S. M. (2014). Influence of rust layers on the corrosion behavior of ultra-high strength steel 300M subjected to wet-dry cyclic environment with chloride and low humidity. Acta Metallurgica Sinica, 28(2), 139-146.

[17] Hameed, A., Zubair, O., Ali Shams, T., Mehmood, Z., Javed, A., & Mehmood, Z. (2020). Failure analysis of a broken support strut of an aircraft landing gear. Engineering Failure Analysis, 117, 104847.

[18] Skubisz, P., & Sinczak, J. (2018). Properties of direct-quenched aircraft forged component made of ultrahigh-strength steel 300M. Aircraft Engineering and Aerospace Technology, 90(5), 713-719.

[19] Daymond, B. T., Binot, N., Schmidt, M. L., Preston, S., Collins, R., & Shepherd, A. (2016). Development of custom 465® corrosion-resisting steel for landing gear applications. Journal of Materials Engineering and Performance, 25(4), 1539-1553.

[20] Bag, A., Delbergue, D., Ajaja, J., Bocher, P., Levesque, M., & Brochu, M. (2020). Effect of different shot peening conditions on the fatigue life of 300 M steel submitted to high stress amplitudes. International Journal of Fatigue, 130, 105274.

[21] Brandstetter, S., Derlet, P. M., Van Petegem, S., Van Swygenhoven, H. (2008). Williamson-Hall anisotropy in nanocrystalline metals: X-ray diffraction experiments and atomistic simulations. Acta Materialia, 56(2), 165-176.

[22] Markmann, J., Yamakov, V., Weissmüller,J. (2008). Validating grain size analysis from X-ray line broadening: A virtual experiment. Scripta Materialia, 59(1):15-18.

[23] Liu, D., Liu, D., Zhang, X., Liu, C., & Ao, N. (2018). Surface nanocrystallization of 17-4 precipitation-hardening stainless steel subjected to ultrasonic surface rolling process. Materials Science and Engineering: A, 726, 69-81.

[24] Galindo-Nava, E. I., & Rivera-Díaz-del-Castillo, P. E. J. (2012). A thermodynamic theory for dislocation cell formation and misorientation in metals. Acta Materialia, 60(11), 4370-4378.

[25] Liu, F. G., Lin, X., Song, M. H., Yang, H. O., Song, K., Guo, P. F., Huang, W. D. (2016). Effect of tempering temperature on microstructure and mechanical properties of laser solid formed 300M steel. Journal of Alloys and Compounds, 689, 225-232.

[26] Holzwarth, U., & Eßzmann, U. (1994). The irreversibility of dislocation-wall formation in persistent slip bands. Philosophical Magazine Letters, 70(2), 75-80.

[27] Rzhavtsev, E. A., & Gutkin, M. Y. (2015). The dynamics of dislocation wall generation in metals and alloys under shock loading. Scripta Materialia, 100, 102-105.

[28] Bag, A., Lévesque, M., & Brochu, M. (2019). Effect of shot peening on short crack propagation in 300M steel. International Journal of Fatigue, 131, 105346.

[29] Kim, J. C., Cheong, S. K., & Noguchi, H. (2013). Evolution of residual stress redistribution associated with localized surface microcracking in shot-peened medium-carbon steel during fatigue test. International Journal of Fatigue, 55, 147-157.

[30] Jeong, I. K., Graf, M. J., & Heffner, R. H. (2005). Effects of Bragg peak profiles and nanoparticle sizes on the real-space pair distribution function. Journal of Applied Crystallography, 38(1), 55-61.

[31] Yin, F., Cheng, G. J., Xu, R., Zhao, K., Li, Q., Jian, J., Hu, S., Sun, S., An, L., & Han, Q. (2018). Ultrastrong nanocrystalline stainless steel and its Hall-Petch relationship in the nanoscale. Scripta Materialia, 155, 26-31.

[32] Armstrong, R. W. (2014). 60 years of Hall-Petch: Past to present nano-scale connections. Materials Transactions, 55(1), 2-12.

[33] Eringen, A. C., & Kim, B. S. (1974). Stress concentration at the tip of crack. Mechanics Research Communications, 1(4), 233-237.

[34] Lee, S. Y., Choo, H., Liaw, P. K., An, K., & Hubbard, C. R. (2011). A study on fatigue crack growth behavior subjected to a single tensile overload: Part II. Transfer of stress concentration and its role in overload-induced transient crack growth. Acta Materialia, 59(2), 495-502.

[35] Yan, W., Fang, L., Sun, K., & Xu, Y. (2007). Effect of surface work hardening on wear behavior of Hadfield steel. Materials Science and Engineering: A, 460-461, 542-549.

[36] Hasnaoui, A. (2003). Dimples on Nanocrystalline Fracture Surfaces As Evidence for Shear Plane Formation. Science, 300(5625), 1550-1552.